Summary: Micro-structured electrode (MSE) arrays allow large area uniform glow discharges to be generated over a wide pressure range up to atmospheric pressure. Electrode widths, thicknesses and distances in the μm-range are realized by means of modern micro machining and galvanic techniques. These electrode dimensions are small enough to generate sufficiently high electric field strengths to ignite gas discharges by applying only moderate radio frequency (RF, 13.56 MHz) voltages (80 V to 390 V in Ne, He, Ar, N_2 and air). The non-thermal plasma system can be characterized by a special probe measuring the electric parameters. MSE driven plasmas demonstrate different behavior from conventional RF or DC discharge plasmas. Due to the very small electrode gap width, *d*, the behavior of the charged particles in the RF field of our system could be described with the DC Townsend breakdown theory. Partially, dependent on the pressure range and type of gas, the breakdown mechanism was dominated by field electron emission or by a high frequency regime. The voltage-current characteristic and electron density of the MSE plasma in He at atmospheric pressure were characteristic for a glow discharge. Using MSE arrays as plasma sources, several applications have been developed and successfully tested including atmospheric pressure plasma chemistry (decomposition of waste gases like CF_4 and NO) and the sterilization of food packaging materials at atmospheric pressure.

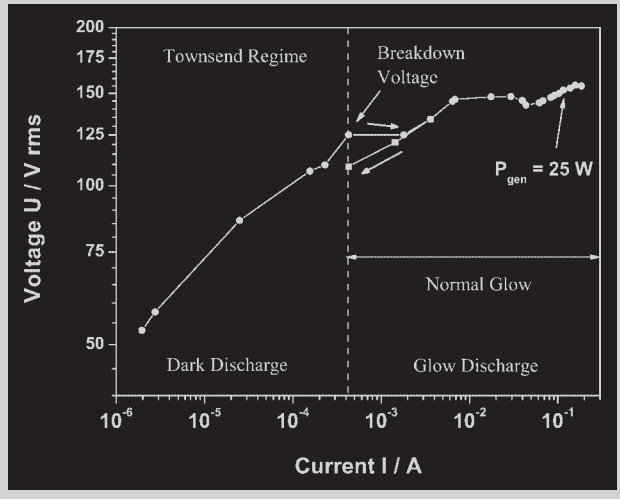

Voltage-current characteristic of a 100 kPa He RF glow discharge generated with an MSE array ($d = 70$ μm).

Micro-Structured Electrode Arrays: Characterization of High Frequency Discharges at Atmospheric Pressure

Lutz Baars-Hibbe,[1] *Philipp Sichler,*[2] *Christian Schrader,*[1] *Karl-Heinz Gericke,*[1] *Stephanus Büttgenbach*[2]

[1] Institut für Physikalische and Theoretische Chemie, Technische Universität Braunschweig Hans-Sommer-Straße 10, D-38106 Braunschweig, Germany
Fax: +49 531 391 5396; E-mail: l.baars-hibbe@tu-bs.de
[2] Institut für Mikrotechnik, Technische Universität Braunschweig Alte Salzdahlumer Str. 203, D-38124 Braunschweig, Germany

Received: August 31, 2004; Revised: December 23, 2004; Accepted: January 5, 2005; DOI: 10.1002/ppap.200400043

Keywords: atmospheric pressure glow discharges (APGD); micro-structured electrode; Paschen curves; radio frequency glow discharges (RFGD); sterilization

Introduction

Non-thermal plasma processing techniques optimized for atmospheric pressure applications have been the subject of recent, growing interest due to their significant industrial advantages. At atmospheric pressure, thin film deposition is possible with very high rates and cost-intensive vacuum technology can be avoided. There have been many approaches published recently to overcome problems in generating and sustaining a stable uniform non-thermal atmospheric plasma.[1–11]

Recently, micro-structured electrode (MSE) arrays have been introduced as alternative atmospheric pressure plasma sources.[12–15] They consist of a system of planar and parallel electrodes (comb structure, see Figure 1) arranged on an insulating substrate and are manufactured by means of modern micro machining and galvanic techniques. The electrode dimensions, especially the electrode gap width, *d*, in the μm-range, are small enough to generate sufficiently high electric field strengths to ignite gas discharges by applying only moderate radio frequency (RF, 13.56 MHz) voltages (less than 400 V).

 DOI: 10.1002/ppap.200400043

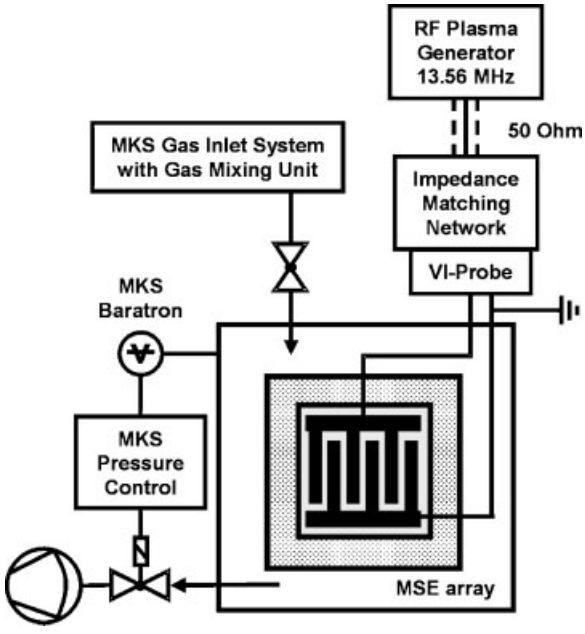

Figure 1. Scheme of the experimental setup. Gas inlet system and vacuum system published in detail in ref.[14]

In the following sections, the breakdown mechanism of the MSE driven radio frequency discharges for two different electrode gap widths (70 μm and 25 μm) are characterized and their special behavior demonstrated, which can be seen to differ from conventional discharges. A voltage-current characteristic in He at atmospheric pressure has been determined and the electron density estimated, in order to classify the MSE plasma as a glow discharge. Additionally, successful applications of the MSE arrays are briefly summarized.

Experimental Part

The MSE arrays have been studied as a non-thermal radio frequency (13.56 MHz) plasma source with the experimental setup shown schematically in Figure 1. The gas inlet system and vacuum system have been described in detail elsewhere.[14] A gas flow rate of 200 sccm was set up by means of mass flow controllers. The discharges were generated using an RF power supply (ENI ACG-3B) equipped with a matching network (ENI MW-5D). The RF generator was power controlled from 0 W to 300 W with steps of 1 W. The generator power, P_{gen}, used to ignite the plasma ranged between 3 W (Ne) and 45 W (N_2). Between the matching network and the MSE array, a special probe (ENI VI-Probe) was inserted in order to measure voltage U, current I, phase angle φ and the effective power, P_{eff}, of the system. The effective powers inserted into the plasma were dependent on the gas chosen and generator power, but were independent of pressure (in the range 10 to 100 kPa).

The MSE arrays were micro-machined nickel structures on a 500 μm thick alumina substrate. The electrode gap design is shown in Figure 2. In order to achieve plasma operation at high-pressure ranges, an electrode thickness up to 100 μm was necessary. Therefore, for 70 μm structures, a 150 μm thick layer of SU8 photo resin was spun on a ceramic wafer already covered with a thin copper layer.[16] The SU8 was prebaked by heating at 373 K. UV-exposure with a chrome mask initiated crosslinking which was then continued on a hotplate. The non-polymerized resin was resolved, leaving a complementary geometry to the desired electrode design. The production of 25 μm MSE arrays was more complicated, because the SU8 mold needed to be stabilized to obtain sufficient quality of the electrode gap structures. Therefore, anchoring structures were integrated into the electrodes. With this design, a thickness of 35 μm could be realized. The electrode width of 1 350 μm and electrode length of 7 200 μm were identical for both structures.

After plating with nickel, most of the SU8 was removed by a long exposure to acetone, and the remaining resin was etched

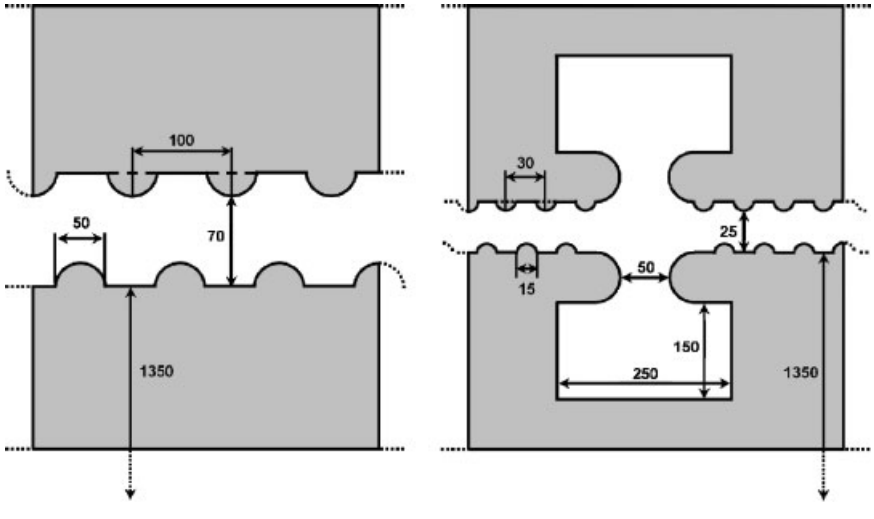

Figure 2. Design of the electrode gaps for the realization of the different MSE gap widths 70 and 25 μm (dimensions in μm).

away by exposure to a CF_4/O_2 plasma. The start layer was etched away with Alketch I+II (Candor Chemie, Bochum, Germany). After cleaning, a 400 nm alumina layer was deposited on the structures to form a protective barrier.

Characterization of the MSE Plasma

The electrode gap had a complex geometry with incorporated protrusions (see Figure 2) allowing the generation of large-area uniform glow discharges in He and Ne at pressures up to 150 kPa and in Ar and N_2 up to 120 kPa.[15] With the 25 μm structures, glow discharges could be generated even in air up to 50 kPa. In order to achieve higher pressures in air, very high applied generator powers (>45W) were necessary to ignite the plasma. Under these conditions, the MSE arrays started to age with the increasing occurrence of sparks over time, finally resulting in destruction by arcing. Non-thermal discharges were generated at the five gaps between the electrodes and, up to 40 kPa, the plasma covered the whole electrode system.[14,15] Using the gases Ne, He and Ar, the plasma burned in all electrode gaps, but with N_2 at a pressure higher than 60 kPa the discharge burned only in one electrode gap. In order to ignite the plasma, an applied generator power of about 3 W in Ne, 5 W in He, a range from 9 W to 22 W in Ar and a range from 18 W to 45 W in N_2 was necessary, depending on the pressure.

In Figure 3 the breakdown voltages (ignition potentials U_{IP}) of the gases Ne, He, Ar and N_2 for an electrode gap width, d, of 70 μm and in the pressure range 10 to 100 kPa are shown.

In order to describe the behavior of the charged particles in the RF field of this system, the DC Townsend breakdown theory was used due to the very small electrode gap width. The motion of the charged particles is drift controlled analogous to DC discharges, because the oscillatory amplitudes of the electrons as well as the ions exceed $d/2$ (35 μm) with

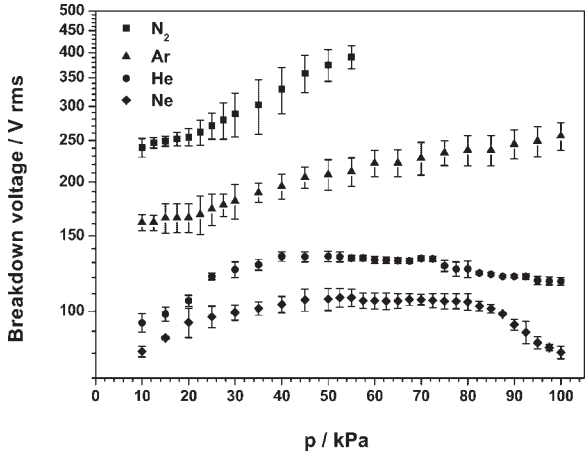

Figure 3. Experimental breakdown voltages in Ne, He, Ar and N_2 ($d = 70$ μm, RF 13.56 MHz, 10–100 kPa).

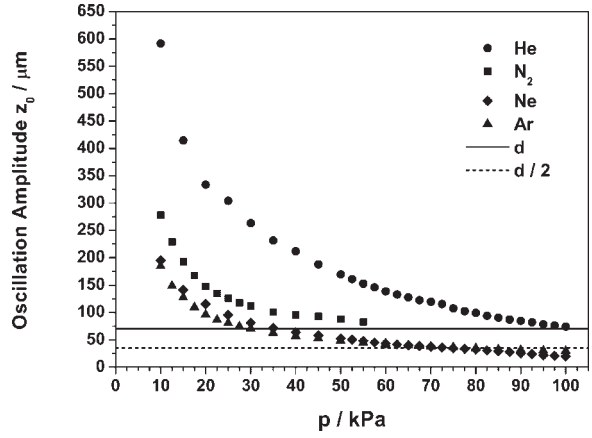

Figure 4. Ion oscillation amplitudes for $d = 70$ μm calculated with the electric field strengths derived from Figure 3.

the exception of Ne and Ar at pressures higher than 80 kPa (see Figure 4).[17] The ion oscillation amplitudes z_0 in Figure 4 were calculated using Equation (1):

$$z_0 = \frac{e \cdot E_0}{m \cdot \omega \cdot \sqrt{\omega^2 + \nu_c^2}} \tag{1}$$

where E_0 is the electric field amplitude, m is the mass of the charged particle, ω is the angular frequency ($2\pi \times$ 13.56 MHz) and ν_C is the e^--neutral collision frequency. Equation (1) gives the extreme values derived from the solution of the equation of motion (Equation (2)) including the pressure dependent Lorentz collisional term in order to regard friction.[18]

$$m \cdot \frac{d^2 z}{dt^2} + m \cdot \nu_c \frac{dz}{dt} = e \cdot E_0 \cdot \sin(\omega \cdot t) \tag{2}$$

The right-hand branches of the Paschen curves of Ar and N_2 and the left-hand branches of Ne and He at pressures higher than 80 kPa obey the Paschen formula derived from the DC Townsend breakdown theory:[19,20]

$$U_{IP} = \frac{B \cdot (p \cdot d)}{C + \ln(p \cdot d)} \tag{3}$$

with

$$C = \ln \frac{A}{\ln\left(1/\gamma + 1\right)} \tag{4}$$

The mentioned branches were fitted with the Paschen formula (curves shown in Figure 5, fitted constants listed in Table 1). The B values of the RF field determined for $d =$ 70 μm are of the same magnitude, but are lower than the B values of the DC field, because the voltages required to initiate and maintain AC discharges decrease strongly, in comparison to DC glow discharges, with increasing frequency.[19,20]

The B value of Ne is much smaller than the DC value, which can partly be explained by the non-matching of the

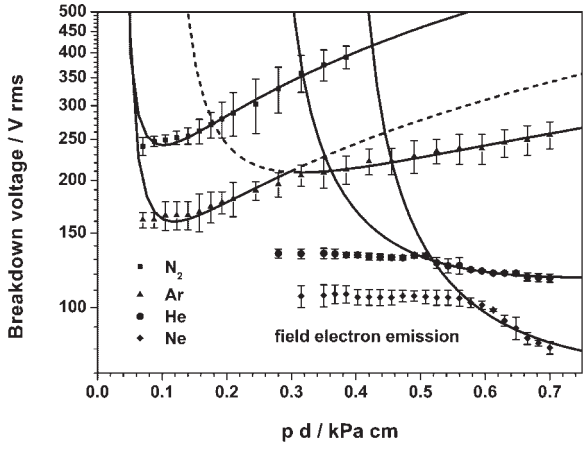

Figure 5. Fitted Paschen curves in Ne, He, Ar and N_2 (electrode gap width $d = 70$ μm).

regions of applicability. At pressures above 80 kPa the ion oscillation amplitudes of Ne do not exceed $d/2$ in the fitted pressure range. Thus, the breakdown controlling regime is a mixture of the high frequency discharge mechanism (also called the α regime) and the Townsend breakdown mechanism, where the high frequency mechanism is dominant.[17,20]

For Ar, the fit over the entire range of 10 to 100 kPa yielded an unsatisfactory result, because the dominant breakdown mechanism changes from the DC Townsend mechanism at low pressures to the high frequency mechanism at high pressures. Analogous to Ne, at pressures above 80 kPa, the ion oscillation amplitudes of Ar do not exceed $d/2$. Thus, the fit range is divided in two parts at the limit given by the DC region of applicability. The B values determined confirm this interpretation, the B value at low pressures even corresponding to the DC B value.

In He at high pressures neither breakdown mechanism is dominant. However, the contribution of the DC Townsend breakdown mechanism is more significant than in Ne, because all amplitudes, z_0, of He exceed $d/2$. Thus, the RF B value of He is higher in relation to the DC B value than in the case of Ne or Ar. These results were confirmed by RF (13.56 MHz) measurements in He performed by Park et al.[7] Park et al. used a capacitor consisting of two planar square electrodes with an electrode gap width varying from 1 000 μm to 9 700 μm. The pressure was varied between 1 kPa and 80 kPa. With electrode distances more than 15 times larger than the MSE gap width (70 μm), the measured breakdown voltages represented the right hand branch of the He Paschen curve (not shown in Figure 5), and the high frequency regime dominated the breakdown mechanism. The authors likewise calculated the oscillation amplitudes of the charged particles, all of which were lower than $d/2$. Additionally, Park et al. found that variation of the electrode material did not result in a significant deviation of the measured breakdown voltages.[7] With a dominating high frequency regime, processes on the surface of the electrodes represented by the secondary electron emission coefficient γ (see below) are negligible. We fitted the data of Park et al. with Equation (3) and obtained a much smaller B value (see Table 1), comparable to the RF B value determined for Ne in relation to the DC B values. In the experiments by Park et al., the He breakdown voltages in the Paschen minimum were lower than 100 V (120 V with $d = 70$ μm). The high frequency regime entirely controlled the breakdown mechanism, resulting in a lowering of the breakdown voltage.

While the Paschen curves for He and Ne fit the experimental data very well at high $p \cdot d$ values, they deviate significantly at lower $p \cdot d$ values (see Figure 5). Theoretically, higher breakdown voltages were expected due to the growing lack of impact partners with decreasing $p \cdot d$ values. Hartherz et al. have shown that with d values in the μm-range, the breakdown voltages are increasingly dominated by field electron emission with decreasing pressure, although the electric field strengths used were less than one magnitude below 10^6 V · cm^{-1} (q. v. below).[19,21]

In Ne and He at pressures lower than 40 kPa, the discharges show a new pressure dependent behavior. As can be

Table 1. Fitted constants of the Paschen formula for two different electrode gap widths, d, and regions of applicability (B and E/p in V · kPa^{-1} · cm^{-1}).

d	Gas	Experiment (RF)			Literature[19] (DC)	
μm		B	C	E_{eff}/p	B	E/p
70	Ne	67.2 ± 4.3	0.92 ± 0.03	110–200	750	750–3 000
1 800	He	32.7 ± 0.6[a)]	0.56 ± 0.04[a)]	10–50[a)]	260	150–1 000
70	He	157.3 ± 2.3	1.28 ± 0.01	170–280	260	150–1 000
70	Ar	661.6 ± 14	2.15 ± 0.03	370–700	1 350	750–4 500
70	Ar	1 356 ± 41	3.14 ± 0.04	700–1 840	1 350	750–4 500
70	N_2	2 378 ± 52	3.28 ± 0.04	1 020–2 820	2 560	750–4 500
25	Ar	1 407 ± 35	3.20 ± 0.03	750–1 770	1 350	750–4 500
25	N_2	2 611 ± 67	3.51 ± 0.03	1 490–3 140	2 560	750–4 500

[a)] B and C calculated from literature data.[7]

seen in Figure 4, in this pressure range the ion oscillation amplitudes of both gases exceeded not only $d/2$ but also d. Thus, the ignition behavior should again be dominated by the DC Townsend breakdown regime. With decreasing pressure, an increasing contribution of the field electron emission additionally lowers the breakdown voltages (significantly only in He). Thus, in the case of He, the voltages measured at low pressures are lower than the expected values given by the Paschen curves fitted at high pressures.

This reason can explain the additional decrease of the breakdown voltage, but not the special pressure dependent behavior shown in this pressure range. The experimental observation of the spatial distribution of the discharge helps with understanding the experimental data. At the breakdown the complete electrode surface is covered with a darker diffuse plasma compared to the intense plasma generated only at the gaps between the electrodes at high pressures. Thus, higher breakdown distances are favored to the shortest electrode gap width of 70 µm. Figure 6 shows that this effect is not only observed with $d = 70$ µm but also with $d = 25$ µm. This is consistent with the observation of additional parasite discharges at pressures lower than 40 kPa, which ignite independently of the MSE discharges within distances of several millimeters inside the chamber. At pressures higher than 35 kPa, the parasite discharges have much higher breakdown voltages than the MSE discharges. The MSE driven discharges of Ne and He at pressures lower than 40 kPa represent the left hand branches of the Paschen curves near the minimum with higher effective d values, d_{eff} (see Figure 7). Therefore, the parasite discharges must represent the right-hand branches of the Paschen curves at high $p \cdot d$ values (shown in Figure 7). In Ne, it was possible to estimate d_{eff}, since with $d_{\mathrm{eff}} > d$ the ion oscillation amplitudes z_0 should not exceed $d_{\mathrm{eff}}/2$, resulting in the high frequency regime dominating the breakdown mechanism. Thus, it is a good approximation to use the fitted constants B and C of Table 1. Table 2 summarizes the estimated d_{eff} values calculated with Equation (3). The solutions $p \cdot d$ are shown in Figure 7. The 1st solution represents the MSE discharges with d_{eff} and the 2nd solution the parasite discharges with d_{eff} equal to the physical shortest distances between the conductors inside the vacuum chamber excluding the MSE array. As expected, with increasing pressure d_{eff} decreases, but the condition $d_{\mathrm{eff}}/2 > z_0$ is always fulfilled (see Figure 4). At pressures higher than 35 kPa, d_{eff} (MSE) becomes equal to d (70 µm). Then, field electron emission dominates the breakdown mechanism (see above). In Ne at a pressure above 30 kPa, parasite discharges are no longer observed, because d_{eff} is smaller than the smallest electrode distance outside the MSE system, resulting in higher breakdown voltages (see above).

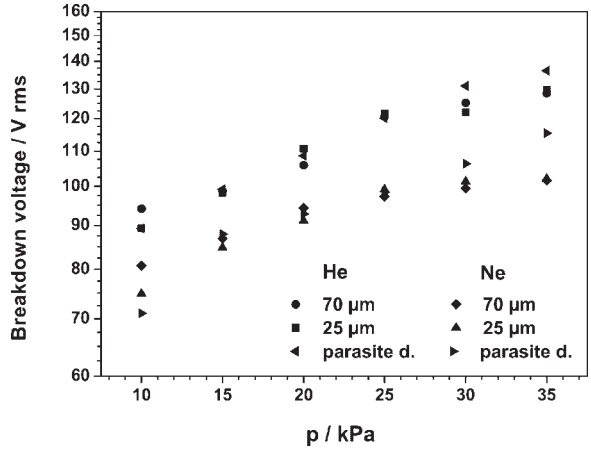

Figure 6. Experimental breakdown voltages in Ne and He of the two different d (70 and 25 µm) and the parasite discharges.

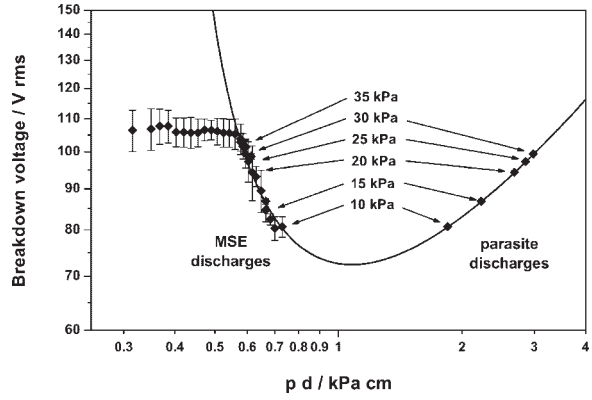

Figure 7. Experimental breakdown voltages in Ne for $d = 70$ µm (10–100 kPa). The $p \cdot d$ values of pressures below 40 kPa were calculated using Equation (3).

Since in He the effective d values were unknown, it was not possible to run a new fit with the Paschen formula, which would result in Paschen curves with considerably lower breakdown voltages than the fitted Paschen curves shown in Figure 5.

With $d = 25$ µm the ion oscillation amplitudes of all gases exceed not only $d/2$ but also d. Thus, the ignition mechanism is dominated by the DC Townsend breakdown regime, which was confirmed by the Paschen fitted constants, B, of Ar and N_2 (see Table 1). However, analogous to the 70 µm prototype, in Ne and He field electron emission dominates the breakdown mechanism at pressures higher than 40 kPa.[22]

Figure 8 compares the RF breakdown voltages of Ar with the DC Paschen curve.[19] Two effects can be observed. With the decrease of d to 25 µm the breakdown voltage is lowered, and with $d = 70$ µm at high pressures the Ar breakdown voltages are higher than the DC breakdown voltages. In Table 3 the estimated experimental secondary electron emission coefficients γ of all gases calculated with Equation (4) are summarized and compared with DC γ and γ_i (electron emission by ion bombardment of the cathode)

Table 2. Estimated effective d values, d_{eff}, for MSE discharges and parasite discharges in Ne. The $p \cdot d$ values were calculated using Equation (3) with $B = 67.2\ V \cdot kPa^{-1} \cdot cm^{-1}$ and $C = 0.92$.

p	U_{IP}	1st solution $p \cdot d$	d_{eff} (MSE)	2nd solution $p \cdot d$	d_{eff} (parasite discharges)
kPa	V	kPa · cm	µm	kPa · cm	µm
10	80.73	0.730	730	1.843	1 843
15	86.83	0.665	443	2.226	1 484
20	94.37	0.617	308	2.680	1 340
25	97.30	0.603	241	2.855	1 142
30	99.43	0.594	198	2.982	994
35	101.63	0.585	167	[a]	[a]

[a] U_{IP} (parasite discharge) is significantly higher than U_{IP} (MSE, $d = 70$ and 25 µm).

values. A higher contribution of γ_i to the ignition, resulting in the lowering of the breakdown voltage, can be excluded, since the calculated ion kinetic energies of Ar have almost identical values at the same $p \cdot d$ values for both electrode distances. Additionally, γ_i of Ar is almost independent of the ion kinetic energies in the range of 5 eV to 500 eV.[23] An increase in the contribution of field electron emission is responsible for this effect, because the ignition electric field strengths more than double. This effect is quantified by an increase in the experimental γ value.

The estimated experimental γ values of $d = 70$ µm confirm the present results, the γ values of Ne and Ar at high pressures being very low compared to the DC value. Thus, the high frequency mechanism dominates. This result can also explain the fact that at high pressures the Ar breakdown voltages are even higher than the DC breakdown voltages (see Figure 8). The lower B value of Ar ($662\ V \cdot kPa^{-1} \cdot cm^{-1}$) cannot compensate for the strong decrease in the γ value. A higher frequency than 13.56 MHz should result in lower breakdown voltages for Ar (see He for comparison).

In order to determine the electron density, n_e, of the RF discharge the voltage-current characteristics were measured in He. Figure 9 shows the voltage-current characteristic of a 100 kPa He RF discharge generated with an MSE array ($d = 70$ µm). The characteristic is similar to the RF discharge characteristics observed by Park et al. (see above).[7,24] Park et al. used a capacitor consisting of two planar square electrodes with an electrode gap width varying from 1 600 µm to 3 200 µm. Since our RF generator was power controlled with steps of 1 W, only five data points were gained before breakdown ($P_{gen} = 5$ W). Thus, no significant voltage drop is observed at breakdown due to the coarse steps. On the other hand, in N_2, a voltage drop of several 10 V is observed.[22] The voltage-current characteristic of N_2 is characteristic for a glow discharge and is very similar to the characteristic of a low pressure DC discharge.[18,22] For both gases the operational range is the normal glow range including the subnormal glow range showing characteristic hysteresis behavior. In He with P_{gen} higher than 7 W, the plasma starts to cover the entire electrode system and the voltage across the discharge (about 150 V) is almost independent of the measured plasma current I_p over several orders of magnitude, which is characteristic for the normal glow range.

The electron density of the RF glow discharge ($P_{gen} =$ 25 W, see Figure 9) was estimated with a simple model used

Table 3. Estimated experimental secondary electron emission coefficients, γ, calculated using Equation (4).

d	Gas	A; literature[19]	C; experiment (RF)	γ	γ_i (E_{kin} range); literature[23] (DC)
µm		$kPa^{-1} \cdot cm^{-1}$			
70	Ne	30.0	0.92 ± 0.03	6.63×10^{-6}	0.12–0.14 (5–90 eV)
1 800	He	22.5	0.56 ± 0.04[a]	2.71×10^{-6} [a]	ca. 0.17 (5–90 eV)
70	He	22.5	1.28 ± 0.01	1.95×10^{-3}	
70	Ar	90.0	2.15 ± 0.03	2.88×10^{-5}	3.4×10^{-2}–3.5×10^{-2} (5–500 eV)
70	Ar	90.0	3.14 ± 0.04	2.10×10^{-2}	
70	N_2	90.0	3.28 ± 0.04	3.53×10^{-2}	4.4×10^{-2} [b]
25	Ar	90.0	3.20 ± 0.03	2.64×10^{-2}	See above
25	N_2	90.0	3.51 ± 0.03	7.33×10^{-2}	4.4×10^{-2} [b]

[a] C and γ calculated from literature data.[7]
[b] γ calculated from literature data.[19]

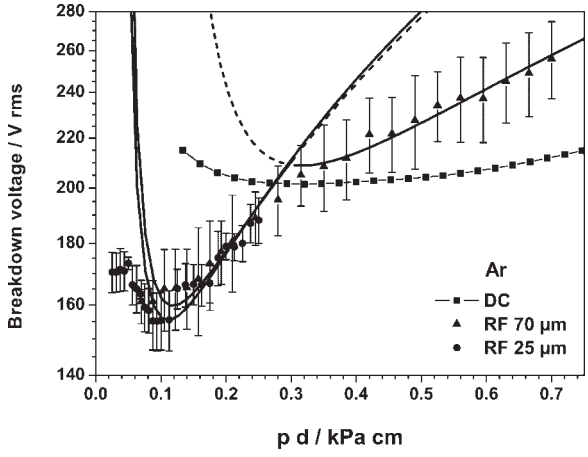

Figure 8. Fitted Paschen curves in Ar. Comparison of the DC breakdown voltages with the experimental RF breakdown voltages of different d.[19] The standard deviation describes the margin of deviation between three manufactured MSE prototypes.

by Park et al., where n_e was calculated according to:

$$\frac{I_p}{A_p} = -n_e \cdot e \cdot \mu_e \cdot E \tag{5}$$

where A_p is the active plasma area and $\mu_e = 0.107\ m^2 \cdot V^{-1} \cdot s^{-1}$ is the electron mobility for He.[24–26] Park et al. measured the sheath thickness of their system with optical emission spectroscopy gaining the thickness of the plasma bulk region in order to estimate the voltage and the electric field strength E across the bulk region.[24] They measured sheath thicknesses of 280 µm to 350 µm ($p = 80$ kPa), dependent on input power, but independent of d. The sheath thickness of Park et al. was at least four times larger than our MSE electrode gap width $d = 70$ µm. Thus, conventional methods to obtain E do not apply to MSE systems. Additionally, the problem of describing how the electric field penetrates the plasma has not yet been solved.[27] In a glow discharge the degree of ionization, x, is very low (see Table 4) and, at high pressures the sheath is collisional. Thus, we estimated the effective electric field strength E by dividing the overall field strength by a factor ε, the measured and pressure dependent dielectric constant of the medium. This effective field strength is probably higher than the actual field strength across the bulk region providing a minimal value of n_e (see Equation (5)). Table 4 summarizes all the estimated values. The degree of ionization ($x \approx 10^{-8}$) as well as the electron density ($n_e \approx 2 \times 10^{17}$ electrons $\cdot$ m^{-3}) are characteristic for a glow discharge.

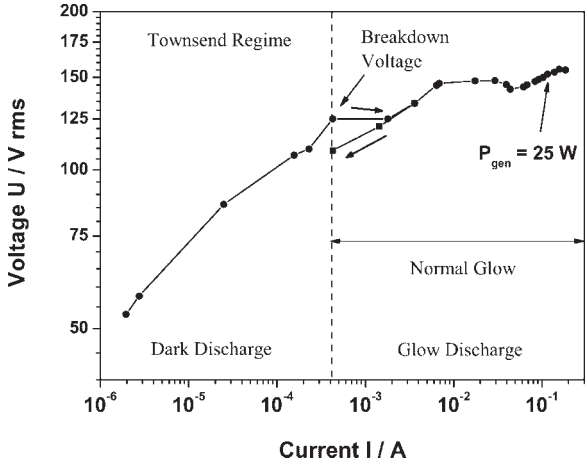

Figure 9. Voltage-current characteristic of a 100 kPa He RF glow discharge generated with an MSE array ($d = 70$ µm).

Table 4. Estimated Debye length, λ_D, in He for pressures 40 to 100 kPa ($d = 70$ µm, $P_{gen} = 25$ W, $P_{eff} = 15$ W). Mean free path length, λ, dielectric constant, ε, of the medium, electron density, n_e, electron temperature, T_e.

p	λ	ε	n_e	Degree of ionization x	T_e	λ_D
kPa	µm		m^{-3}		eV	µm
40	0.490	1.482	1.30×10^{17}	1.34×10^{-8}	1	21
					5	46
					20	92
50	0.392	1.469	1.77×10^{17}	1.46×10^{-8}	1	18
					5	40
					20	79
60	0.327	1.358	1.97×10^{17}	1.35×10^{-8}	1	17
					5	38
					20	75
70	0.280	1.182	1.26×10^{17}	7.42×10^{-9}	1	21
					5	47
					20	94
80	0.245	1.201	1.80×10^{17}	9.24×10^{-9}	1	18
					5	39
					20	78
90	0.218	1.199	2.22×10^{17}	1.01×10^{-8}	1	16
					5	35
					20	71
100	0.196	1.132	2.30×10^{17}	9.45×10^{-9}	1	16
					5	35
					20	69

With pressures of 40 kPa to 60 kPa, the degree of ionization, x, is independent of pressure, because in this pressure range the breakdown mechanism is dominated by field electron emission (see above). At a pressure of 70 kPa, the transition of the breakdown mechanism causes a decrease of x. On the other hand, in the Paschen minimum (at pressures higher than 80 kPa) the breakdown voltage decreases (see Figure 3), which partially compensates the decrease in x resulting in a minimum of x at 70 kPa.

With n_e it is possible to estimate the Debye shielding distance, λ_D, representing the minimum sheath thickness.[18] λ_D is calculated according to:

$$\lambda_D = \sqrt{\frac{\varepsilon_0 \cdot k \cdot T_e}{e^2 \cdot n_e}} \tag{6}$$

where ε_0 is the permittivity of a vacuum, k is the Boltzmann constant and T_e is the electron temperature. The MSE

plasma source generates electrons with kinetic energies of more than 20 eV.[14] It is not possible to measure an electron energy distribution function with a conventional Langmuir probe. The smallest probe size of about 10 μm (realized by means of modern micro machining techniques) is still of the same magnitude as the electrode gap width. Although the experimental realization itself is an interesting challenge, the probe would disturb the measurement results by influencing the plasma parameters, because the ratio of plasma volume to probe surface is too small. Additionally, the special ratio of λ_D, r_{probe} and the mean free path length λ would necessitate developing a new model for data analysis.[25] Thus, in Table 4 we have summarized the λ_D values for three different T_e in each case. The estimated values of λ_D (with $T_e = 5$ eV) are too high for λ_D to represent the minimum sheath thickness. The actual electron densities are probably higher (see above) resulting in smaller λ_D values. At a pressure of 100 kPa, $n_e \approx 10^{18}$ electrons $\cdot$ m^{-3} yields $\lambda_D = 17$ μm ($T_e = 5$ eV) resulting in a 36 μm thick plasma bulk region for $d = 70$ μm. An electron density n_e of 10^{18} electrons $\cdot$ m^{-3} is high, but still characteristic for a glow discharge and was confirmed by simulations done at atmospheric pressure in He.[18,28] λ_D is more than one order of magnitude higher than λ and of the same magnitude as the thickness of the bulk plasma, as well as the electrode gap width d. These ratios are very different from conventional DC or RF systems. λ_D increases with decreasing pressure. At pressures below 40 kPa λ_D exceeds d, but not d_{eff} (see Table 2 for comparison), increasing the complexity of the system. In order to discuss the role of λ_D in stabilizing the plasma against sparking or the influence of λ_D on other effects, a new model needed to be developed for our system. With P_{gen} up to 40 W in He, no sparking is observed. Additionally, it has to be considered that the sheath will expand and contract due to the oscillating electric field.[27] In the future, we intend to measure the sheath thickness directly with optical emission spectroscopy in order to confirm the estimated values of λ_D. With additional experiments it will be possible to develop a comprehensive model providing acceptable quantitative predictions.

Applications

With the MSE array as a plasma source incorporated into a micro-reactor, the decomposition of the greenhouse gas CF_4 was performed with rates of over 90% at a pressure of 10 kPa in He and N_2. At atmospheric pressure, the abatement rate was still over 70%.[15,28] Additionally, the decomposition of NO in 100 kPa He has been investigated, where an abatement rate of 70% was achieved.[15,29]

The MSE plasma source generates electrons with high kinetic energies (see above), fluorescent excited atoms and ions.[14] These species have shown their applicability as sterilizing agents for resistant spores at atmospheric pressure.[30] In sterilization experiments, the thermo-resistant spores of the vegetative bacteria *Bacillus cereus* and the UV-resistant spores of the fungus *Aspergillus niger* were deactivated in He and Ar. The setup consisted of the MSE plasma source coplanarly arranged opposite an inoculated (10^6 spores of each microorganism in 50 μL spore-solution) substrate (Si, Cu or different plastic films). The substrate was biased with various potentials to accelerate the reactive plasma species towards the substrate. After the plasma exposition, the substrate was pressed on the spore specific medium to detect viable spores. Optical emission spectroscopy proved the presumption that accelerated electrons and ions are the dominating sterilizing agents, because in the sterilizing UV range below 300 nm no emission lines were detected.[31]

Conclusion

With the MSE array, an alternative atmospheric pressure plasma source has been identified with many applications, such as in plasma chemistry (decomposition of waste gases like CF_4) and the sterilization of food packaging materials.

The MSE driven radio frequency discharges showed special behavior, which differed from conventional high frequency gas discharges. Due to the very small electrode gap width (25 μm to 70 μm) the behavior of the charged particles in the RF field could be described with the DC Townsend breakdown theory. Partially, dependent on pressure range and gas, the breakdown mechanism was dominated by field electron emission or the high frequency regime. The voltage-current characteristic and electron density of the MSE plasma in He at atmospheric pressure were characteristic of a glow discharge. The MSE system was very complex and could not be described quantitatively with a simple model derived from other RF or DC model systems. Additional experiments are necessary in order to develop a model which will provide acceptable quantitative predictions. Nevertheless, with the knowledge gained it is possible to design MSE arrays optimized for different pressure ranges and gases given by the application.

Acknowledgements: This work was partially supported by the *Bundesministerium für Bildung und Forschung* (bmb + f), Germany, under contract No. 03D0070B/6. We also wish to thank our project partners Dr. *T. R. Dietrich* and *A. Freitag* of mgt mikroglas technik AG.

[1] F. Massines, P. Ségur, N. Gherardi, C. Khamphan, A. Ricard, *Surf. Coat. Technol.* **2003**, *174–175*, 8.
[2] S. Okazaki, M. Kogoma, M. Uehara, Y. Kimura, *J. Phys. D: Appl. Phys.* **1993**, *26*, 889.

[3] D. Trunec, A. Brablec, J. Buchte, *J. Phys. D: Appl. Phys.* **2001**, *34*, 1697.
[4] K. Kelly-Wintenberg, A. Hodge, T. C. Montie, L. Deleanu, D. Sherman, J. R. Roth, P. P. Tsai, L. Wadsworth, *J. Vac. Sci. Technol.* **1999**, *17*, 1539.
[5] US 5,403,453 (1995), invs.: J. R. Roth, P. P. Tsai, L. Wadsworth, C. Liu, P. D. Spence.
[6] US 5,414,324 (1995), invs.: J. R. Roth, P. P. Tsai, C. Liu, M. Laroussi, P. D. Spence.
[7] J. Park, I. Henins, H. W. Herrmann, G. S. Selwyn, *J. Appl. Phys.* **2001**, *89*, 15.
[8] R. H. Stark, K. H. Schoenbach, *J. Appl. Phys.* **1999**, *85*, 2075.
[9] C. Penache, A. Bräuning-Demian, L. Spielberger, H. Schmidt-Böcking, ''*Proc. of the 7th Intern. Symp. on High Pressure Low Temp. Plasma Chem. (HAKONE VII)*'', Greifswald 2000, p. 501.
[10] J. G. Eden, S.-J. Park, N. P. Ostrom, S. T. McCain, C. J. Wagner, B. A. Vojak, J. Chen, C. Liu, P. von Allmen, F. Zenhausern, D. J. Sadler, C. Jensen, D. L. Wilcox, J. J. Ewing, *J. Phys. D: Appl. Phys.* **2003**, *36*, 2869.
[11] I. Radu, R. Bartnikas, M. R. Wertheimer, *J. Phys. D: Appl. Phys.* **2003**, *36*, 1284.
[12] C. Geßner, P. Scheffler, K.-H. Gericke, ''*Proc. of the 7th Intern. Symp. on High Pressure Low Temp. Plasma Chem. (HAKONE VII)*'', Greifswald 2000, p. 112.
[13] C. Geßner, P. Scheffler, K.-H. Gericke, ''*Proceedings of the International Conference on Phenomena in Ionized Gases (XXV ICPIG)*'', Nagoya 2001, p. 151.
[14] K.-H. Gericke, C. Geßner, P. Scheffler, *Vacuum* **2002**, *65*, 291.
[15] L. Baars-Hibbe, P. Sichler, C. Schrader, C. Geßner, K.-H. Gericke, S. Büttgenbach, *Surf. Coat. Technol.* **2003**, *174–175*, 519.
[16] J. O'Brien, P. J. Hughes, M. Brunet, B. O'Neill, J. Alderman, B. Lane, A. O'Riordan, C. O'Driscoll, *J. Micromech. Microeng.* **2001**, *11*, 353.
[17] K. Wiesemann, ''*Einführung in die Gaselektronik*'', B. G. Teubner, Stuttgart 1976, p. 267.
[18] J. R. Roth, ''*Industrial Plasma Engineering*'', IOP Publishing, Bristol 1995, p. 418.
[19] Yu. P. Raizer, ''*Gas Discharge Physics*'', Springer Verlag, Berlin 1997, p. 133.
[20] A. Grill, ''*Cold Plasma in Materials Fabrication*'', IEEE Press, New York 1994, p. 24.
[21] P. Hartherz, ''*Anwendung der Teilentladungsmeßtechnik zur Fehleranalyse in festen Isolierungen unter periodischer Impulsspannungsbelastung*'', Ph.D. thesis, Darmstadt 2002, ISBN 3-8322-0413-X.
[22] L. Baars-Hibbe, P. Sichler, C. Schrader, N. Lucas, K.-H. Gericke, S. Büttgenbach, *J. Phys. D: Appl. Phys.* **2005**, *38*, 510.
[23] S. C. Brown, ''*Basic Data of Plasma Physics*'', MIT Press, Cambridge 1966, p. 219.
[24] J. Park, I. Henins, H. W. Herrmann, G. S. Selwyn, *J. Appl. Phys.* **2001**, *89*, 20.
[25] G. Janzen, ''*Plasmatechnik*'', Hüthig, Heidelberg 1992, p. 40.
[26] A. V. Phelps, J. L. Pack, L. S. Frost, *Phys. Rev.* **1960**, *117*, 470.
[27] R. N. Franklin, *J. Phys. D: Appl. Phys.* **2003**, *36*, R309.
[28] P. Sichler, S. Büttgenbach, L. Baars-Hibbe, C. Schrader, K.-H. Gericke, *Chem. Eng. J.* **2004**, *101*, 465.
[29] P. Scheffler, C. Geßner, K.-H. Gericke, ''*Proc. of the 7th Intern. Symp. on High Pressure Low Temp. Plasma Chem. (HAKONE VII)*'', Greifswald 2000, p. 407.
[30] L. Baars-Hibbe, C. Schrader, P. Sichler, T. Cordes, K.-H. Gericke, S. Büttgenbach, S. Draeger, *Vacuum* **2004**, *73*, 327.
[31] C. Schrader, P. Sichler, L. Baars-Hibbe, N. Lucas, A. Schenk, K.-H. Gericke, S. Büttgenbach, S. Draeger, *Surf. Coatings Technol.*, in press.

